Proliferating droplets formed via prebiotic polymerisation: the missing link between chemistry and biology on the origin of life

Muneyuki Matsuo
Hiroshima University
Kensuke Kurihara (kkurihara@jamstec.go.jp)
Japan Agency for Marine-Earth Science & Technology (JAMSTEC)

Article

Keywords: origin-of-life, polymers, peptide generation, peptide-based material development.

Posted Date: September 1st, 2020

DOI: https://doi.org/10.21203/rs.3.rs-65297/v1

Abstract

The hypothesis that prebiotic molecules were transformed into polymers that evolved into proliferating molecular assemblages and eventually a primitive cell was first proposed about a hundred years ago. However, no proliferating model prebiotic system has yet been realised because different conditions are required for polymer generation and self-assembly of polymers. In this study, we identified conditions suitable for concurrent peptide generation and self-assembly, and we showed how a proliferating peptide-based droplet could be created by using synthesised amino acid thioesters as prebiotic monomers. Oligopeptides generated from the monomers spontaneously formed droplets through liquid–liquid phase separation in water. The droplets underwent a steady growth–division cycle by periodic addition of monomers through autocatalytic self-reproduction. Heterogeneous enrichment of RNA and lipids within droplets enabled RNA to protect the droplet from dissolution by lipids. These results provide experimental platforms for origin-of-life research and open up novel directions in peptide-based material development.

Background

Construction in a laboratory of a model protocell, which is an artificial supramolecular system that expresses the essential properties of life, would be an important step in defining life and exploring the origin of life[1,2]. According to the chemical evolution scenario suggested by Oparin and Haldane in the 1920s[3,4], a protocell is a proliferating coacervate droplet (CD). According to an abiogenesis scenario, a CD is formed from organic molecules via liquid–liquid phase separation (LLPS)[5] and results mainly from the spontaneous assembly of oppositely charged molecules or from hydrophobic polymers and, in particular, of prebiotic polymers or oligomers. Although there has been a report of a CD[5] that expresses a higher-order function, which is a function that are not expressed by the molecule alone but are expressed through intermolecular interactions affects the properties of molecular aggregates, by encapsulation of the main constituents of living organisms (i.e., RNA, lipids, and peptides), no CD has yet been constructed that induces interactions among its constituents that lead to self-reproduction, i.e., reproduction that takes place from within the closed boundary of the structure itself. In none of the foregoing hypotheses has there been an experimental proof of how the molecular assemblies formed by the primitive molecules came to proliferate. Experimental proof of proliferation by simple physical mechanisms, independent of molecular species, would therefore be an important milestone in the maturation of scenarios on the origin of life. CDs have been produced experimentally at room temperature and under ambient atmospheric pressure conditions using peptides generated at high temperatures or pressures that mimicked the volcanic conditions prevalent in the primordial Earth in previous studies[6,7]. Recent studies have reported the formation of novel CDs composed of oligonucleotides[8], phospholipids[9], or oligopeptides[10] in aqueous solutions. Renewed interest in the role of CDs in the origin of life has been generated by the novel studies of Mann and co-workers, who have demonstrated cellular life-like features such as communication[11] and predator–prey interactions[12] in populations of CDs. As is the case with CD formation, autocatalytic self-reproduction is a crucial property of protocells that proliferate steadily[13] and has been demonstrated for supramolecular structures such as DNA origami rafts[14,15], lipid micelles[16–18],

and lipid vesicles[19–21] in an aqueous medium. Previous studies of the fusion and division of molecular assemblies without self-reproduction have reported the importance of non-equilibrium states[22–24]. However, few studies have reported recursive self-reproduction of supramolecular assemblies in response to periodic stimuli[25] because metastable assemblies tend to move toward equilibrium. Under present conditions, the dynamics of self-maintenance by cellular organisms—the property of maintaining an almost constant state vis-a-vis external stimuli via intrinsic response mechanisms—requires not only self-reproduction but also recursiveness under conditions of cyclic stimulation[26,27]. For example, the division of cyanobacterial cells is synchronized with the light–dark cycle of Earth's rotation[28], and L-form bacteria proliferate by membrane destabilisation caused by excessive membrane production and repeated perturbations from the environment, e.g., water flow[29,30]. Self-reproduction and periodic stimuli may have played crucial roles that enabled recursive proliferation (i.e., growth and division through self-reproduction) of prebiotic supramolecular assemblies on primitive Earth. The proliferation of molecular assemblies through self-reproduction is a "biological" property specific to organisms and has not been observed in viruses that sophisticated supramolecular assemblies. The formation of polymers from monomers and of molecular assemblies from polymers are common "chemical" property in nature and are based on interactions such as covalent bonding and intermolecular forces. The creation of proliferating CDs via such mechanisms, however, has not been achieved at all. The problem of mimicking this step of chemical evolution in the origin of life has never been solved experimentally during the roughly hundred years since it was first proposed[1,2]. In principle, a CD can self-reproduce only if the conditions are satisfied for reproduction of both the CD itself and the peptides, which are the CD building blocks. In previous CD studies, peptides that are constituents of CDs have been produced in an elaborate manner via organic synthesis under volcanic conditions, biosynthesis or solid-phase synthesis. CDs have then been formed by the produced peptides under mild aqueous conditions[6–12].

To emerge a proliferating droplet with prebiotic polymerisation, we constructed an autocatalytic self-reproducing liquid–liquid phase-separated (LLPS) droplet that was inspired by de Duve's "thioester world" hypothesis, which argues that prebiotic peptides might have been generated from amino acid thioesters under mild aqueous conditions[31]. We were able to simultaneously form LLPS droplets and generate peptides by using a designed and synthesised thioesterified cysteine derivative as a monomer precursor for the spontaneous oligomerisation of an amino acid thioester under mild aqueous conditions. A continuous supply of a monomer precursor that kept the LLPS droplet in a non-equilibrium state enabled the LLPS droplets to undergo a steady growth–division cycle that maintained droplet size while increasing the number of droplets. We also showed that the LLPS droplets were able to resist dissolution by lipids and to maintain themselves when nucleic acids and lipids were both present in them if the concentrated nucleic acids were localised in the inner boundary of the LLPS droplet with the assistance of generated peptides. Overall, we were able to demonstrate how a novel proliferating droplet protocell could be formed by the oligomerisation of amino acid thioesters and functionalised by oligonucleotides (Fig. 1). Such a protocell could have served as a link between "chemistry" and "biology" during the origin of life. This study may serve to explain the emergence of the first living organisms on primordial Earth.

Results

Spontaneous formation of droplets from amino acid thioesters. We designed a monomer **M** that was capable of producing peptides and facilitating the self-assembly of molecules under aqueous conditions sufficiently mild to allow formation of droplets and self-reproduction of the building blocks of **M** (Fig. 2a). A monomer with a thioester and unprotected cysteine group at its C- and N-terminus, respectively, would be expected to polymerise spontaneously in water. Therefore, to provide **M** while reducing with dithiothreitol (DTT) in subsequent experiments, a disulfide precursor of **M** ($\mathbf{M}_{\mathbf{pre}}$) was synthesised (Figs. S1–S3). The C-terminus of **M** was capped with a benzyl mercaptan (BnSH) leaving group.

The reduction of the $\mathbf{M}_{\mathbf{pre}}$ disulfide by DTT in water generated two **M** molecules, which then reacted spontaneously to yield peptides (Fig. 2a). To confirm the formation of droplets, we monitored turbidity as a function of time and recorded microscopic images of an aqueous solution containing $\mathbf{M}_{\mathbf{pre}}$ and DTT (Figs. 2b, c). Five minutes after addition of $\mathbf{M}_{\mathbf{pre}}$ (5 mg, 10 mM) and DTT (4 mg, 25 mM) to deionised water, the turbidity began to increase, and it continued to increase for 16 h (Figs. 2b and c [red line]). The increase in turbidity suggested the formation of molecular self-assemblies in solution. We therefore examined the solution under a differential interference contrast (DIC) microscope to confirm the formation of molecular self-assemblies induced by a series of reactions after addition of $\mathbf{M}_{\mathbf{pre}}$ (Fig. 2d and Supplementary Movie 1). No molecular self-assemblies were observed within the first 5 min after mixing the $\mathbf{M}_{\mathbf{pre}}$ and DTT reagents; however, micrometre-sized molecular self-assemblies appeared after 1 h. Twenty-seven hours after mixing, the spherical molecular self-assemblies had grown and were present in significant numbers. Furthermore, DIC microscopy revealed that fusion of the molecular self-assemblies (Supplementary Movie 2) had begun 1 h after addition of $\mathbf{M}_{\mathbf{pre}}$. The spherical shapes maintained by the fused assemblies suggested that the formed aggregates were droplets.

To confirm that the reduction of $\mathbf{M}_{\mathbf{pre}}$ induced the development of turbidity in the solution containing both $\mathbf{M}_{\mathbf{pre}}$ and DTT, the solution was observed in real time with a microscope, and the turbidity of a sample of the solution dispensed every hour from the initial solution was measured. When $\mathbf{M}_{\mathbf{pre}}$ was dissolved in deionised water in the absence of DTT, no molecular assemblies larger than 1 μm were observed under a DIC microscope, although smaller assemblies resulted in the development of slight turbidity (Figs. 2c [green line] and S4a). Moreover, the turbidity was close to zero when DTT was dissolved in water because DTT is soluble in water (Fig. 2c [blue line]). In contrast to the dispersed reaction solution after addition of thioesterified cystine $\mathbf{M}_{\mathbf{pre}}$ and DTT, no turbidity was observed when cystine was mixed with cysteine dihydrochloride, BnSH, and DTT (Figs. S4b, c) because the molecular self-assemblies did not disperse, and the aggregates precipitated in a similar way with the addition of only cystine to water (Fig. S4d). These results confirmed that droplet formation resulted from thioester-induced reactions. To clarify the contribution of the cysteine moiety in the monomers to droplet formation, we also synthesised thioesterified glycine (Gly-SBn) (Methods, Fig. S5) by a protocol similar to the synthesis of $\mathbf{M}_{\mathbf{pre}}$ (Fig. S1). There was no turbidity in an aqueous solution containing Gly-SBn and DTT either 5 min or 24 h from its preparation (Fig. S6). These results indicated that the reduction of the disulfide precursor with DTT and

the subsequent chemical reaction at the thioester site and the cysteine side chain of $\mathbf{M}_{pre}$ were essential for spontaneous droplet formation. The pH range for droplet formation was at least 3–11 (Fig. S7).

Oligomerisation-induced self-assembly of liquid–liquid, phase-separated droplets via autocatalysis. To verify that oligomerisation was induced at the thioester site and the cysteine side chain of **M**, we allowed mixing of $\mathbf{M}_{pre}$ (10 mM) with DTT (25 mM) to reduce $\mathbf{M}_{pre}$ and oligomerise the generated **M** in deionised water. The product was separated from the droplet dispersion. The reaction solution was lyophilised to remove water and BnSH, and the white powder residue was washed with acetonitrile to remove unreacted and oxidised DTT (Figs. 3a, S8). The obtained powder was analysed by proton nuclear magnetic resonance (^{1}H NMR) (Fig. S9a) and electrospray ionisation mass spectrometry with a time-of-flight mass spectrometer (ESI-TOF-MS). Comparison of oligopeptide spectra with those of $\mathbf{M}_{pre}$ (Fig. S9b) showed that the peak of the benzene ring (peak a in Fig. S9b) and the peaks near the disulfide (peaks b and c in Fig. S9b) had almost disappeared, whereas an amide proton (d) was newly detected. The mean degree of polymerisation of the obtained powder was estimated from the ratio of the areas of the peaks at 8.8 ppm and 4.8 ppm in Fig. S9a to be 4.1. Each peak was assigned to the proton of terminal amine groups and amide bonds, respectively. In addition, the mass-to-charge ratios observed in the ESI-TOF-mass spectra revealed degrees of polymerisation of 2 to at least 4 in the reaction solution 24 h after mixing $\mathbf{M}_{pre}$ and DTT (Fig. S10). The intensities of the monomer and dimer decreased from their initial values, whereas the intensity of the trimers and tetramers tended to increase. These results indicated that $\mathbf{M}_{pre}$ was reduced by DTT to yield **M**, which then formed at least di-, tri-, and tetrapeptides.

To clarify the contribution of the generated oligopeptide to droplet formation, products except biproducts (BnSH and oxidized DTT), were purified from the solution 24 h after mixing $\mathbf{M}_{pre}$ and DTT, and its ability to form a droplet was investigated (Table in Fig. 3a). The solutions that contained no oligopeptides or BnSH did not become turbid, whereas those containing both oligopeptides and BnSH were dispersed, and the formation of spherical molecular assemblies in them was apparent under a DIC microscope (Fig. S11). The indication that oligomerisation-induced self-assembly had occurred in these mixtures strongly suggested that the association of oligopeptides and BnSH components was essential for LLPS-droplet formation. We therefore concluded that the droplets were formed by associative LLPS[32]. The fact that the terminus of the peptide has an ammonium cation and that BnSH has a benzene ring suggests that the droplet may be an associative LLPS caused by cation–π interactions. Indeed, it was reported that LLPS droplets in vivo were formed due to cation-π interactions between lysine residues with an ammonium cation and other amino acids residues with an aromatic ring in the protein side chain[33].

The $\mathbf{M}_{pre}$ residual proportion, i.e., the proportion of the primary amines that was not involved in peptide formation, was determined from the amount of primary amine $\mathbf{M}_{pre}$ that was consumed (Fig. 3b), which was estimated by the fluorescamine method (Fig. S12a). The rate of formation of droplets was calculated from the changes of the areas of the peaks corresponding to benzene ring protons in the ^{1}H NMR spectrum of the solution (Fig. S12b). The decrease of the $\mathbf{M}_{pre}$ residual proportion (Fig. S12c) was consistent with the observed increase of the droplet formation rate (Fig. 3b). The curve of the droplet

formation rate was sigmoidal and was fit to the autocatalytic reaction equation using the Levenberg–Marquardt method on the assumption that the reaction was autocatalytic (Fig. S13). The autocatalytic nature of the peptide synthesis was confirmed by the observation that the shape of the curve of the $\mathbf{M_{pre}}$ residual proportion also became sigmoidal (Fig. 3c) when the amount of DTT added was decreased to reduce the reaction rate. However, the curve of the droplet formation rate was sigmoidal even though the amount of added DTT did not change because the droplet formation rate was controlled by the rate of decomposition of $\mathbf{M_{pre}}$, and it increased at a slower rate than the rate of decrease of the $\mathbf{M_{pre}}$ residual proportion. These results indicated that LLPS droplets were formed autocatalytically, and a hypothesis that the droplets themselves served as sites of peptide generation.

Recursive self-reproduction of LLPS droplets. To demonstrate the continuous growth of the droplets upon serial additions of $\mathbf{M_{pre}}$ and DTT, we measured the changes in the size distribution of the droplets that formed after each addition. Figure 4a shows the predicted size distributions of LLPS droplets after repeated additions of $\mathbf{M_{pre}}$ and DTT. After the first addition of $\mathbf{M_{pre}}$, the droplet size distribution was expected to shift fully to the right as the droplets grew. This expectation was confirmed by the continuous increase in the size of the LLPS droplets revealed by the droplet size analysis (Fig. 4b). This result indicated that nanometre-sized molecular aggregates were formed during the first five minutes after mixing of the $\mathbf{M_{pre}}$ and DTT. After five minutes, they grew or fused to become large enough to be observed with a microscope.

Upon subsequent addition of $\mathbf{M_{pre}}$ and DTT into the dispersion containing the LLPS droplets, the droplet size distribution was expected to change into one of two patterns, depending on the region of oligomerisation in the droplets (Fig. 4a, right). Two possible cases were considered. In the first case, if new droplets formed spontaneously in the solution as oligomerisation proceeded, then a new peak at a smaller size would appear in the corresponding distribution (Fig. 4a, upper right). In the second case, if oligomerisation occurred inside or at the interface of the LLPS droplets, the pre-existing LLPS droplets would grow larger, and no new LLPS droplets would be generated because no oligopeptides would be available in the solution. No separate peak would therefore appear in the size distribution (Fig. 4a, lower right). In the second case, some oligopeptides would also be generated outside and then incorporated into the existing LLPS droplets. To identify the actual oligomerisation site, we added equal volumes of $\mathbf{M_{pre}}$ and DTT to 1 mL of LLPS droplet dispersion 24 h after the first addition of $\mathbf{M_{pre}}$ (10 mM) and DTT (25 mM), and we then monitored the temporal evolution of the size distribution of the LLPS droplets (Fig. 4c). The sizes of the existing LLPS droplets increased with time, and no additional peak corresponding to newly formed LLPS droplets was detected. This result strongly supported the hypothesis that oligomerisation occurred inside or at the interface of the LLPS droplets: that is, these findings pointed to autocatalytic self-reproduction of the LLPS droplets due to the ability of LLPS droplets to serve as active sites for oligopeptide generation.

The LLPS droplets formed in the current study self-reproduced recursively while they were continuously nourished by consumption of $\mathbf{M_{pre}}$ and were extruded as a means of periodic dilution to induce shearing

(Fig. 4d). In particular, the LLPS droplets grew and fused by autocatalytic self-reproduction and then divided upon addition of $\mathbf{M_{pre}}$ and DTT (Fig. 4e). To quantitatively evaluate the recursive growth and division of the LLPS droplets, we analysed the temporal evolution of the average diameter of LLPS droplets in the dispersion. We monitored the droplet population over six periods: the initial droplet-formation period and five cycles of $\mathbf{M_{pre}}$ addition to the existing, uniformly sized droplets (nutrient, white triangles in Fig. 4e) and extrusion using a syringe (shear, black triangles in Fig. 4e). During each cycle, we observed an increase in the size of the LLPS droplets stimulated by addition of $\mathbf{M_{pre}}$ and DTT that was followed by a decrease in size upon extrusion. From the second to the sixth period, the particle size at the beginning and end of a cycle was almost the same, and the mode of particle size development also remained approximately unchanged. Referencing the time-course analysis of the droplet size in Fig. 4e, a significant correlation exceeding the 95% confidence interval (light blue zone in Fig. S14a) was found at the 33rd lag, which corresponds to the time immediately after the nutrient was taken in. This result clearly indicated that there was a high autocorrelation between particle size changes in every cycle. Use of DIC microscopy also revealed similar recursive patterns of LLPS droplet diameters (Figs. S14b, c). The consistency up to 3 h after mixing $\mathbf{M_{pre}}$ and DTT between the increase in average droplet size (Fig. 4e) and the rate of droplet formation to the one third (Fig. 3b) (correlation coefficient = 0.96) strongly suggested that the increase in droplet size mainly depended on the chemical reaction at the initial stage. However, the fact that the correlation coefficient between the two experiments more than 3 hours after mixing decreases extremely to 0.068 suggested that the droplets generated by the reaction grew by the fusion dominantly (Fig. S15). However, the fact that no significant increase in particle size was observed when only water was added to the extruded droplet dispersion (Fig. S16) indicated that the increase in particle size at the initial stage was not due to the fusion of droplets after extrusion but instead was an effect of the reaction. The fact that almost the same size of the droplets reached a steady state during every period therefore meant that the number density of droplets, despite the effect of dilution, was kept constant by the addition of precursors. These results demonstrated that LLPS droplets underwent a recursive growth–division process, that is proliferation, in response to the external stimuli of nutrient addition and extrusion.

Nucleic acid/lipid concentration in droplets. In the origin of life, a simpler prebiotic polymer[34,35] might have provided a scaffold for peptide-droplets formation before the synthesis of the common major components of current organisms, i.e. nucleic acids, lipids and proteins. However, to evolve into the ancestors of all modern organisms, proliferating peptide-CDs require to cooperate with these major components[36–38]. The absence of such a CD up to the present has led to a gap between the three major scenarios—the “RNA world”[39], “lipid world”[40], and “protein world”[41]—each of which envisions that a self-reproducing system of the corresponding molecules has evolved into a proliferating protocell via interactions with other molecules. We therefore tested the ability of the droplets created in this study to serve as active sites to incorporate and concentrate fluorescence-tagged nucleic acids and lipids into a droplet (Fig. 5a). Twenty-four hours after mixing $\mathbf{M_{pre}}$ and DTT, 6-carboxy-tetramethylrhodamine (TAMRA)-tagged RNA (TAMRA-RNA) and boron-dipyrromethene (BODIPY)-tagged phospholipid (BODIPY-lipid) solutions were added to the droplet dispersion. The droplets were then observed with a confocal

laser scanning (CLS) microscope. No fluorescence emission from the droplets was observed two minutes after addition of the RNA and lipid solutions. Thirty minutes after addition, however, the molecular assembly gradually began to emit fluorescence derived from TAMRA and BODIPY, and that fluorescence continued for 360 min (Fig. 5b). Line profiles of the fluorescence intensity (Fig. 5c–f) were generated from each fluorescence channel image of the LLPS droplets (Fig. 5b, bottom row). The time-course of the line profiles confirmed the gradual incorporation of RNA oligomers and phospholipids into the LLPS droplets after simultaneous addition of these molecules (Figs. 5c, e). In the case of RNA, the maximum fluorescence was detected near the inner boundaries of the droplet, whereas the fluorescence peaked at the centre of the droplet in the case of the lipids. A comparison of the CLS microscopy images of the LLPS droplets during independent incorporation of the RNA oligomers or lipids with the corresponding line profiles (Figs. 5d, f) revealed positions of fluorescence intensity peaks similar to the peak positions when TAMRA-RNA (Figs. 5d, g) or BODIPY-lipid (Figs. 5f, h) was added separately to the different droplet dispersions. To show that this experiment was not affected by the fluorophore itself, we confirmed that the results were similar for experiments labelled with different fluorophores. Similar distributions of fluorescence intensity were detected for RNA, phospholipids, and DNA labelled with alternative fluorescent probes. Fluorescence derived from fluorescein isothiocyanate-tagged RNA (FITC-RNA) or DNA and TAMRA-tagged DNA (TAMRA-DNA) were detected along the inner boundary of the droplet (Figs. S18a–c), and the fluorescence of Texas Red–tagged phospholipids (Texas Red–lipid) was detected around the centre of the droplet (Fig. S18d). The interactions between nucleic acids, lipids, and peptides generated spatial heterogeneity between the RNA and lipids in the same LLPS droplet. These results implied that the droplets were heterogeneous, with a gradual hydrophilic boundary and a hydrophobic centre that were composed mainly of oligopeptides and BnSH, respectively. Raman microspectrometry revealed that the droplets were composed of a relatively hydrophobic central part with a relatively large Bn/water ratio and of a relatively hydrophilic peripheral part with a relatively small Bn/water ratio (Fig. S19).

When only phospholipids were added, their surfactant effect resulted in a reduction in the size of the droplets (Figs. 5h, f); however, no significant decrease of droplet size was observed upon addition of RNA and lipid (Figs. 5b, c, e) or of RNA (Figs. 5d, g). This result suggested that the incorporation of nucleic acids enabled the proliferating droplet to maintain its size despite the perturbation associated with lipid addition. To confirm that the self-maintenance ability associated with the incorporation of nucleic acids was ubiquitous, we mixed the droplet dispersion with a TAMRA-RNA solution and BODIPY-lipid dispersion or with RNase-free water, followed by a 24-h incubation and fluorescence-activated cell sorting (FACS) analysis. Population analysis of the FACS data after addition of either fluorescence-labelled RNA or fluorescence-labelled lipids indicated that the fluorescence intensity, which corresponded to the amount of RNA or lipids incorporated by the droplet, increased in both cases, and that the width value of forward scattering pulse, which corresponds to the droplet size, decreased only when lipid was added (Fig. S20). These results strongly suggested that RNA suppressed any reduction of particle size upon lipid addition. Collectively, these results indicated that the localisation of RNA oligomers near the interface of the droplets contributed to the self-maintenance of the droplets. Raman spectroscopy revealed that the

hydrophobic ratio was higher in the centre of the droplet than in the periphery of the droplet that contained the non-fluorescent labelled nucleic acids and lipids (Fig. S21). Compared with the droplets without addition of biomolecules (Fig. S19), it was suggested that the water inside the droplets was replaced by hydrophilic DNA and amphiphilic phospholipids. The heterogeneity of the internal structure of the droplet led to the self-maintenance of the droplet, because the nucleic acid was localised in the peripheral part of the droplet, where it contributed to the undercoat structure. The possibility that this localisation was caused by size exclusion as well as by the hydrophilic/hydrophobic balance of inner molecules cannot be dismissed.

To evaluate the effects of oligopeptides on the incorporation and concentration of hydrophilic RNA oligomers and amphiphilic (rather than hydrophobic) phospholipids into the BnSH phases that could be regarded as a main component of the droplet centre, we measured the decrease in the fluorescence intensities of aqueous TAMRA-RNA or BODIPY-lipid solutions layered for 24 h over the BnSH solution via high-sensitivity fluorescence spectroscopy with photon-counting detectors. The fluorescence intensity in the aqueous phase decreased in both the TAMRA-RNA solution and BODIPY-lipid solution (Fig. S22a), but there was a difference between the two in the magnitude of the decrease of fluorescence in the presence of the oligopeptides (Figs. S22a, c). In the case of the TAMRA-RNA solution, the fluorescence intensity in the presence of the oligopeptides was less than one-third the intensity in the absence of the oligopeptides, whereas in the case of the BODIPY-lipid solution, there was little difference in the fluorescence intensity in the presence or absence of the oligopeptides. A similar result was obtained when the fluorescence moiety was changed (Figs. S22b, d). These results indicated that RNA oligomers and phospholipids were not only incorporated but also concentrated in the BnSH phases, and that oligopeptides could further enhance the RNA enrichment of the droplets because of the high permeability of the membraneless structure of the LLPS droplets.

Discussion

The LLPS droplets that we produced under mild conditions were capable of thioester reaction–induced compartmentalisation, autocatalytic self-reproduction, a steady growth–division cycle, macromolecular enrichment, and self-maintenance. Peptide formation and accompanying droplet formation are necessary but not sufficient to ensure that a droplet can proliferate because self-reproduction—the production of components of the droplet by the droplet itself—is also indispensable. In the case of the current LLPS droplets, proliferation could be realised by physicochemical interactions without specific molecular recognition.

A physical autocatalytic reaction, which is induced by an equilibrium shift due to incorporation of products into formed molecular aggregates, is one kind of autocatalytic reaction[16–19]. More important, however, for the realisation of a self-reproducing system that would generate protocells, is a concentration-induced autocatalysis (CiA) reaction: an autocatalytic reaction made possible by the molecular assemblies of substrates and catalysts formed by the reaction. Examples include the self-reproduced liposomes reported in previous studies[20,21]. A CiA system is a self-reproducing system

because the components of the molecular assembly are generated in the molecular assemblage. In the system described here, CiA could occur because of the gradual accumulation of monomers with a hydrophilic cysteine moiety and a hydrophobic benzyl mercaptan moiety into droplets with an amphiphilic gradient and a membraneless structure. Although autocatalytic reactions that lead to self-replication (i.e., reactions that lead to construction of an identical copy of the system) of RNA or peptides generally require specific complementary molecular recognition, CiA can be induced by non-specific intermolecular interactions, but only to the extent of phase separation. For this reason, self-reproduction of prebiotic polymers by CiA based on molecular phase behaviour must have played as important a role as LLPS in the emergence of a protocell that was a simple cellular organism in a primitive environment where intermolecular interactions were inefficient enough to cause autocatalytic reactions based on specific molecular recognition.

The proliferation of the LLPS droplets was consistent with the thioester world scenario and demonstrated that peptide formation via thioester reactions could have facilitated the formation of CD-based protocells on the primitive Earth. Therefore, we consider the viability of the molecules used in the current study in a prebiotic environment. Monomer **M** was a thioester of cysteine and BnSH. In a prebiotic environment, thioesters can be synthesized at near neutral pH through metal oxidation[42]. Moreover, thioesters have been proposed to function as energy currency in primitive metabolism because they can receive energy from the electron transport system and deliver it to ADP for ATP synthesis independent of membrane structure in the current electron transport system[43]. They may also have contributed to the self-production of primitive cells. Syntheses of cysteine and cystine have been attempted by Sagan et al. under more-or-less prebiotic conditions in a reductive environment that are skeptical at the present[44], but their prebiotic synthesis pathways are currently unknown[45]. BnSH is a model hydrophobic thiol. An alkylthiol, for example, would be a good prebiotic candidate for a hydrophobic thiol[46]. In contrast to the primitive Earth environment, oxygen was abundant under our experimental conditions. The precursor $\mathbf{M}_{pre}$, which was a cross-linkage of two **M** monomers, was therefore reduced with DTT as a reductant model to provide **M** in water. This system could therefore be regarded as a model system that mimicked the emergence and proliferation of protocells under the following prebiotic scenario.

Hydrophobic thiols and amino acids, including cysteine, were produced and created an organic soup at high temperature, high pressure, and either highly acidic or very basic conditions in a geyser. Organic soups emanating from geysers formed ponds on Earth and yielded thioesters by metal oxidation on the surfaces of minerals[47]. The thioester monomers polymerised spontaneously, and the products of polymerisation underwent phase separation to form droplets. With the intermittent flow of organic soup from the geyser, the droplets would have proliferated via dilution, shearing, and incorporation of nutrients. As mentioned above, primitive cells would have flourished around the geyser, and thioesters would have been the main metabolic agent.

These proliferating droplets composed of peptides could serve as containers to integrate the RNA, lipid and peptide during the early history of Earth because the droplets not only incorporated nucleic acids and

lipids but also acquired the ability to survive by accelerating interactions among these constituents such as expression of the homeostasis of particle size. Droplets such as those used in this study must have concentrated various substrates and formed a hydrophobic reaction field, which may have contributed to the formation of reaction networks as well as the synthesis of lipids, nucleic acids, and peptides. The nucleic acids in such reaction networks may have provided a useful roadmap that led to the emergence of an information system. The concentrations of nucleic acids and lipids formed by the gentle amphiphilic gradient in droplets facilitated performance of physicochemical roles by the nucleic acids as follows. The concentrated RNA protected the droplets from dissolution by lipids because the hydrophilic RNA was localised near the inner interface of the droplet by the amphiphilic gradient.

In addition, the nucleic acids accumulated inside the assembled droplet could have concentrated other potential substrates and catalytic molecules in a process called hyperconcentration via electrostatic interactions or hydrogen bonding. Nucleic acids could have functioned as information carriers to control the self-reproduction process. Self-reproduction induced by hyperconcentration has been reported in vesicles[48–50]. If the nucleic acids concentrated within the present droplets altered the self-reproduction behavior of the droplets by collecting molecules around the droplets, it is likely that the droplet functioned as a carrier of information that affected the rates of survival and proliferation. Because this polymer was distributed to newly formed droplets, droplets enriched with polymers and other molecules would have acquired genetic information via hyperconcentration. LLPS droplets carrying genetic information could have generated the universal ancestor by combining proliferation with advanced phenomena[51] such as self-propulsion[52,53], droplet–droplet communication[11] and competition[12]. To construct a more life-like droplet such as active/dissipative droplets[54–56], it is necessary to release the internal products through the interaction reaction of these biomolecules through those dynamics.

In summary, because the process of evolution from amino acid thioesters to the universal ancestor could be realised by concentration of RNA, lipids and peptides inside a proliferating droplet and a subsequent expression of a biological-like function, it is no exaggeration to call this scenario as mentioned above the “droplet world”. Various life-like functions can be imparted to a droplet by inserting alternative amino acids or peptides between cysteine and the thioester moiety in the current monomer or by using other alkylthiols as leaving groups. Interestingly, non-ribosomal peptide synthesis using a similar mechanism has also been discovered in some bacteria and eukaryotic cells[57,58]. In these in vivo peptide syntheses, amino acid thioesters function as monomers to form peptides. Droplets that are composed of peptides and nucleic acids, and formed inside a cell can serve as sites of reactions related to gene expression in modern cells[59,60]. These results are consistent with the scenario that the protocell was based on CDs formed by thioester reactions. Furthermore, since this droplet world hypothesis was derived from model experiments, it also implies that a protocell may emerged by CiA-polymerization of more primitive monomers[34,35] than the amino acid thioesters. The system proposed in this study is therefore a very powerful platform not only for verifying the ancient droplet world scenario of the origin of life but also for developing self-sustainable materials that mimic superior forms of life.

Methods

Synthesis of 3,3'-disulfanediylbis(1-(benzylthio)-1-oxopropan-2-ammonium) dichloride ($(Cys\text{-}SBn)_2$•2HCl, M_{pre}). *N,N'*-Di(*tert*-butoxycarbonyl)-L-cystine [$(Boc\text{-}Cys\text{-}OH)_2$] (4.4 g, 10 mmol) was activated by mixing *N,N'*-dicyclohexylcarbodiimide (DCC, 4.5 g, 2.2 eq.), 1-hydroxybenzotriazole (HOBt, 3.4 g, 2.2 eq.) and *N,N*-diisopropylethylamine (DIEA, 7.7 mL, 6.6 eq.) in dichloromethane. The solution was stirred for 10 min at 0 °C. After addition of benzyl mercaptan (BnSH, 5.2 mL, 6.6 eq.) to the solution, the mixture was stirred for 12 h at 25 °C. The reaction solution was filtered and evaporated under reduced pressure. The obtained crude product was purified by MPLC (hexane/ethyl acetate (4/1, v/v)) and then high-performance liquid chromatography (HPLC) (chloroform) to obtain a clear oil product $(Boc\text{-}Cys\text{-}SBn)_2$ in 48% yield. The purified product was identified as $(Boc\text{-}Cys\text{-}SBn)_2$ based on its ^{1}H NMR (Fig. S2) and electrospray ionisation time of flight mass spectrometry (ESI-TOF MS) spectra. The obtained $(Boc\text{-}Cys\text{-}SBn)_2$ (653 mg, 1 mmol) was added to 5 mL of 4N HCl/ethyl acetate and stirred at 25 °C for 2 h. After filtration, the residue was washed with ethyl acetate and then dried to obtain the product as a white powder in 92% yield. The product was identified as $(Cys\text{-}SBn)_2$•2HCl (M_{pre}) via ^{1}H NMR (Fig. S3), ^{13}C NMR, and ESI-TOF MS measurements. ^{1}H NMR (400 MHz, DMSO-d_6) δ = 8.87(6H, s), 7.50–7.00 (10H, m), 4.70–4.48 (2H, brd), 4.27 (4H, s), 3.27–3.00 (4H, m). ^{13}C NMR (400 MHz, DMSO-d_6) δ = 194.59, 136.52, 128.78, 128.48, 127.35, 99.37, 57.55, 32.69, 32.49. ESI-TOF-MS(MeOH) *m/z* = 489.0818 ($[M + H]^+$ C20H25N2O2S4 required 489.0560).

Synthesis of 2-(benzylthio)-2-oxoethan-1-ammonium chloride [(Gly-SBn)•HCl]. *N'*-(*tert*-butoxycarbonyl)-L-glycine (Boc-Gly-OH, 876 mg, 5 mmol) was activated by mixing *N,N'*-dicyclohexylcarbodiimide (DCC,1135 mg, 1.1 eq.), 1-hydroxybenzotriazole (HOBt, 743 mg, 1.1 eq.) and *N,N*-diisopropylethylamine (DIEA, 1.9 mL, 3.3 eq.) in dichloromethane. The solution was stirred for 10 min at 0 °C. After addition of benzyl mercaptan (BnSH, 1.3 mL, 3.3 eq.) to the solution, the mixture was stirred for 12 h at 25 °C. The reaction solution was filtered and evaporated under reduced pressure. The obtained crude product was purified by medium-pressure liquid chromatography (hexane/ethyl acetate (19/1, v/v)) and then HPLC (chloroform) to obtain a clear oil product Boc-Gly-SBn. The purified product was identified as Boc-Gly-SBn via the spectra of ^{1}H NMR and ESI-TOF-MS. The obtained Boc-Gly-SBn (703 mg, 2.5 mmol) was added to 4N HCl/ethyl acetate 6 mL and stirred at 25 °C for 2 h. After filtration, the residue was washed with ethyl acetate and then dried to obtain the product as a white powder in 87 % yield. The product was identified as [(Gly-SBn)•HCl] via ^{1}H NMR measurement and ESI-TOF MS measurement. ^{1}H NMR (400 MHz, CD_3OD) δ = 7.40–7.20(5H, m), 4.27 (2H, s), 4.10 (4H, s). ESI-TOF-MS (MeOH) *m/z* = 182.0654 ($[M + H]^+$ C9H12NOS required 182.0634). The NMR spectrum is shown in Fig. S5.

Microscopic observations. M_{pre} (5 mg, 10 mmol) and/or the reductant DTT (4 mg, 25 mmol) were added to 1 mL of deionised water and shaken for 15 s. Aqueous solutions (25 µL) were placed on a glass plate, and the plate was then immediately covered with a cover glass using a Frame-Seal^{TM} incubation chamber (9 mm × 9 mm, 25 µL, Bio-Rad Laboratories, Inc.) as a spacer. Bright field images were obtained

with differential interference contrast microscopy. Fluorescence microscopic images were obtained with a confocal microscope fitted with a 488-nm excitation laser and a band path (BP) 525/50 nm emission filter, or a 561-nm excitation laser and a BP 609/54 nm emission filter.

Particle size distribution measurement by dynamic light scattering. The sizes of droplet were measured at 25 °C with an ELSZ-1000 particle analyser, which is suitable for the measurement of particle sizes from 0.6 nm to 10 μm. A 50-μL sample of aqueous mixtures was placed in a quartz cuvette and equilibrated to 25°C prior to measurements. The distribution of aggregate sizes was measured every 30 min for 24 h.

Reaction monitoring via NMR spectroscopy. M_{pre} (11 mg, 20 mmol) and DTT (8 mg, 50 mmol) were added to heavy water (2 mL) and vortexed for 15 s at room temperature. The resulting solution was aliquoted into NMR tubes (500 μL) and measured every 10 min for 24 h.

Reaction-monitoring by fluorescence spectroscopy. M_{pre} (11 mg, 20 mmol) and DTT (8 mg, 50 mmol) were added to water (2 mL) in a microtube and then vortexed for 15 s at room temperature. The prepared M_{pre} solution (20 μL) and fluorescamine solution (90 μL) in super-dehydrated dimethyl sulfoxide (15 mg / 2.5 mL) were mixed. Immediately after mixing, 90 μL of phosphate buffer solution was added, and then the microtube was flicked five times gently. The mixed solution was incubated for 30 min, and then 100 μL of the solution was dispensed into a quartz cell and measured via a fluorescence spectrometer. This procedure was conducted at each point in time for monitoring purposes. The rate of consumption of primary amine was calculated from the changes in absorbance at 476 nm and equated to the monomer conversion rate.

Additional methods. Additional methods were explained as Supplementary Methods in Supplementary Information.

Declarations

Acknowledgements

The authors thank Prof. Taro Toyota of The University of Tokyo for his enlightening comments on this work. This work was financially supported by the Okazaki ORION project of the Exploratory Research Centre on Life and Living Systems (ExCELLS) and by Japan Society for the Promotion of Science Grants-In-Aid for Scientific Research (KAKENHI) (grant numbers JP17H04876 and JP15K17850). Additional financial support was provided by a grant from the Yoshida Scholarship Foundation; the Kurita Water and Environment Foundation (15E011, 16E018, 18D007, 19K011); the Oil & Fat Industry Kaikan; Kao Foundation for Arts and Sciences; The Public Foundation of Chubu Science and Technology Centre; The Hori Sciences and Arts Foundation; a Grant-in-aid for the Graduate School of Integrated Science for Life, Hiroshima University; and the “Innovation inspired by Nature” Research Support Program of Sekisui Chemical Co. Ltd. The Raman microscopy and spectrometry were performed by the Division of Instrumental Analysis, Research Support Centre, Institute for Research Promotion, Kagoshima University.

This work also received technical and official support from the Functional Genomics Facility of the National Institute for Basic Biology Core Research Facilities; the Instrument Centre of the Institute of Molecular Science; and Prof. Satoshi Nakata of Hiroshima University.

Competing interests:

The authors declare no competing financial interests.

Author contributions:

K.K. and M.M. designed the experiments. M.M. performed the experiments, analysed the data, and prepared the draft. K.K. and M.M. wrote the manuscript.

References

1. Rasmussen, S. *et al. Protocells: Bridging Nonliving and Living Matter*. 712 (The MIT Press, 2008).
2. Capra, F. & Luisi, P. L. *The systems view of life: A unifying vision*. (Cambridge University Press, 2014).
3. Oparin, A. I. *The origin of life*. Proiskhozhdenie Zhizni, lzd. Moskovskiy Rabochiy (1924) translation by Ann Synge. In: *The origin of life.* (ed. Bernal, J. D.) 199–234 (Weidenfeld and Nicholson, 1967).
4. Haldane J. B. S. Origin of life. *The Rationalist Annual* **148**, 3–10 (1929).
5. Koga, S. et al. Peptide–nucleotide microdroplets as a step towards a membrane-free protocell model. *Nature Chemistry* **3**, 720–724, doi:10.1038/nchem.1110 (2011).
6. Fox, S. W., Harada, K. & Kendrick, J. Production of spherules from synthetic proteinoid and hot water. *Science* **129**, 1221–1223, doi:10.1126/science.129.3357.1221-a (1959).
7. Fox, S. W. Thermal polymerisation of amino-acids and production of formed microparticles on lava. *Nature* **201**, 336–337, doi:10.1038/201336a0 (1964).
8. Marras, A. E., Vieregg, J. R., Ting, J. M., Rubien, J. D. & Tirrell, M. V. Polyelectrolyte complexation of oligonucleotides by charged hydrophobic—neutral hydrophilic block copolymers. *Polymers* **11**, doi:10.3390/polym11010083 (2019).
9. Wang, M. & Wang, Y. Development of surfactant coacervation in aqueous solution. *Soft Matter* **10**, 7909–7919, doi:10.1039/c4sm01386g (2014).
10. Tang, T. Y. D., Antognozzi, M., Vicary, J. A., Perriman, A. W. & Mann, S. Small-molecule uptake in membrane-free peptide/nucleotide protocells. *Soft Matter* **9**, 7647–7656, doi:10.1039/c3sm50726b (2013).
11. Joesaar, A. *et al.* DNA-based communication in populations of synthetic protocells. *Nature Nanotechnology* **14**, 369–378, doi:10.1038/s41565-019-0399-9 (2019).
12. Qiao, Y., Li, M., Booth, R. & Mann, S. Predatory behaviour in synthetic protocell communities. *Nature Chemistry* **9**, 110–119, doi:10.1038/nchem.2617 (2017).

13. Gánti, T. *The Principles of Life.* (Oxford University Press, 2003).
14. Kim, J., Lee, J., Hamada, S., Murata, S. & Ha Park, S. Self-replication of DNA rings. *Nature Nanotechnology* **10**, 528–533, doi:10.1038/nnano.2015.87 (2015).
15. He, X. *et al.* Exponential growth and selection in self-replicating materials from DNA origami rafts. *Nature Materials* **16**, 993–997, doi:10.1038/nmat4986 (2017).
16. Bachmann, P. A., Luisi, P. L. & Lang, J. Autocatalytic self-replicating micelles as models for prebiotic structures. *Nature* **357**, 57–59, doi:10.1038/357057a0 (1992).
17. Morrow, S. M., Colomer, I. & Fletcher, S. P. A chemically fuelled self-replicator. *Nature Communications* **10**, doi:10.1038/s41467-019-08885-9 (2019).
18. Post, E. A. J. & Fletcher, S. P. Controlling the kinetics of self-reproducing micelles by catalyst compartmentalisation in a biphasic system. *The Journal of Organic Chemistry* **84**, 2741–2755, doi:10.1021/acs.joc.8b03149 (2019).
19. Walde, P., Wick, R., Fresta, M., Mangone, A. & Luisi, P. L. Autopoietic self-reproduction of fatty acid vesicles. *Journal of the American Chemical Society* **116**, 11649–11654, doi:10.1021/ja00105a004 (1994).
20. Takahashi, H. *et al.* Autocatalytic membrane-amplification on a pre-existing vesicular surface. *Chemical Communications* **46**, 8791–8793, doi:10.1039/c0cc02758h (2010).
21. Matsuo, M. *et al.* A sustainable self-reproducing liposome consisting of a synthetic phospholipid. *Chemistry and Physics of Lipids* **222**, 1–7, doi:10.1016/j.chemphyslip.2019.04.007 (2019).
22. 10.1038/ncomms10658
Yin, Y. *et al.* Non-equilibrium behaviour in coacervate-based protocells under electric-field-induced excitation. *Nature Communications* **7**, Article number: 10658, doi: 10.1038/ncomms10658 (2016).
23. Lu, T. & Spruijt, E. Multiphase Complex Coacervate Droplets. *Journal of the American Chemical Society* **142**, 2905–2914, doi:10.1021/jacs.9b11468 (2020).
24. Nakashima, K. K., Baaij, J. F., & Spruijt, E. Reversible Generation of Coacervate Droplets in an Enzymatic Network. *Soft Matter* **14**, 361–367, doi:10.1039/c7sm01897e (2018).
25. Kurihara, K. *et al.* A recursive vesicle-based model protocell with a primitive model cell cycle. *Nature Communications* **6**, doi:10.1038/ncomms9352 (2015).
26. Szostak, J. W., Bartel, D. P. & Luisi, P. L. Synthesizing life. *Nature* **409**, 387–390, doi:10.1038/35053176 (2001).
27. Zhu, T. F. & Szostak, J. W. Coupled growth and division of model protocell membranes. *Journal of the American Chemical Society* **131**, 5705–5713, doi:10.1021/ja900919c (2009).
28. Martins, B. M. C., Tooke, A. K., Thomas, P. & Locke, J. C. W. Cell size control driven by the circadian clock and environment in cyanobacteria. *Proceedings of the National Academy of Sciences of the United States of America* **115**, 11415–11424, doi:10.1073/pnas.1811309115 (2018).
29. Leaver, M., Domínguez-Cuevas, P., Coxhead, J. M., Daniel, R. A. & Errington, J. Life without a wall or division machine in Bacillus subtilis. *Nature* **457**, 849–853, doi:10.1038/nature07742 (2009).

30. Errington, J. L-form bacteria, cell walls and the origins of life. *Open biology* **3**, 120143, doi:10.1098/rsob.120143 (2013).
31. de Duve, C. *Blueprint for a cell: the nature and origin of life.* (Carolina Biological Supply Co: Neil Patterson, 1991).
32. Martin, N. Dynamic synthetic cells based on liquid-liquid phase separation. *ChemBioChem* **20** 2553–2568, doi:10.1002/cbic.201900183 (2019).
33. Saito, M. *et al.* Acetylation of intrinsically disordered regions regulates phase separation. *Nature Chemical Biology* **15**, 51–61, doi:10.1038/s41589-018-0180-7 (2019).
34. Mamajanov, I., Caudan, M., & Jia, T. Z. Protoenzymes: The case of hyperbranched polymer-scaffolded ZnS nanocrystals. *Life* **10**, 150, doi:10.3390/life10080150 (2020).
35. 10.1073/pnas.1902336116
Jia, T. Z. *et al.* Membraneless polyester microdroplets as primordial compartments at the origins of life. *Proceedings of the National Academy of Sciences* **116**, 15830–15835, doi: 10.1073/pnas.1902336116 (2019).
36. Lee, D. H., Granja, J. R., Martinez, J. A., Severin, K. & Ghadiri, M. R. A self-replicating peptide. *Nature* **382**, 525–528, doi:10.1038/382525a0 (1996).
37. Andras, P. & Andras, C. The origins of life – the 'protein interaction world' hypothesis: protein interactions were the first form of self-reproducing life and nucleic acids evolved later as memory molecules. *Medical Hypotheses* **64**, 678–688, doi:10.1016/j.mehy.2004.11.029 (2005).
38. Guseva, E., Zuckermann, R. N. & Dill, K. A. Foldamer hypothesis for the growth and sequence differentiation of prebiotic polymers. *Proceedings of the National Academy of Sciences of the United States of America* **114**, 7460–7468, doi:10.1073/pnas.1620179114 (2017).
39. Gilbert, W. Origin of life: The RNA world. *Nature* **319**, 618. doi:10.1038/319618a0 (1986).
40. Segre, D., Ben-Eli, D., Deamer, D. W. & Lancet, D. The lipid world. *Origins of Life and*
41. *Evolution of the Biosphere* **31**, 119–145, doi:10.1023/A:1006746807 (2001).
42. Dyson, F. J. A model for the origin of life. *Journal of Molecular Evolution* **18**, 344–350, doi:10.1007/BF01733901 (1982).
43. Camprubi E., Jordan S. F., Vasiliadou R., & Lane N. Iron catalysis at the origin of life. *IUBMB Life.* **69**, 373–381, doi:10.1002/iub.1632 (2017).
44. Alberts, B. *et al. Molecular Biology of the Cell Sixth Edition* (W. W. Norton & Company, 2014).
45. Khare, B. & Sagan, C. Synthesis of cystine in simulated primitive conditions. *Nature* **232**, 577–579, doi:10.1038/232577a0 (1971).
46. Parker, E. T. *et al.* Primordial synthesis of amines and amino acids in a 1958 Miller H_2S-rich spark discharge experiment. *Proceedings of the National Academy of Sciences of the United States of America* **108**, 5526–5531, doi: 10.1073/pnas.1019191108 (2011).
47. Huber, C. & Wächtershäuser, G. Activated acetic acid by carbon fixation on (Fe,Ni)S under primordial conditions. *Science* **276**, 245–247, doi:10.1126/science.276.5310.245 (1997).

48. Mulkidjanian, A. Y. *et al.*, Origin of first cells at terrestrial, anoxic geothermal fields, *Proceedings of the National Academy of Sciences of the United States of America* **109**, E821-E830, doi: 10.1073/pnas.1117774109, (2012).
49. Kurihara, K. *et al.* Self-reproduction of supramolecular giant vesicles combined with the amplification of encapsulated DNA. *Nature Chemistry* **3**, 775–781, doi:10.1038/nchem.1127 (2011).
50. Matsuo, M. *et al.* DNA length-dependent division of a giant vesicle-based model protocell. *Scientific Reports* **9**, doi:10.1038/s41598-019-43367-4 (2019).
51. Matsuo, M. *et al.* Environment-sensitive intelligent self-reproducing artificial cell with a modification-active lipo-deoxyribozyme. *Micromachines* **11**, 606, doi.org/10.3390/mi11060606 (2020).
52. Hanczyc, M. Droplets: unconventional protocell model with life-like dynamics and room to grow. *Life* **4**, 1038–1049, doi:10.3390/life4041038 (2014).
53. Hanczyc, M., Toyota, T., Ikegami, T., Packard, N. & Sugawara, T. Fatty acid chemistry at the oil-water interface: self-propelled oil droplets. *Journal of the American Chemical Society* **129**, 9386–9391, doi:10.1021/ja0706955 (2007).
54. Toyota, T., Maru, N., Hanczyc, M. M., Ikegami, T. & Sugawara, T. Self-propelled oil droplets consuming "fuel" surfactant. *Journal of the American Chemical Society* **131**, 5012–5013, doi:10.1021/ja806689p (2009).
55. 10.1038/s41467-018-04488-y
Tena-Solsona, M. *et al.* Self-selection of dissipative assemblies driven by primitive chemical reaction networks. *Nature Commununications* **9**, 2044, doi:10.1038/s41467-018-04488-y (2018).
56. Parrilla-Gutierrez, J. M. *et al.* Adaptive artificial evolution of droplet protocells in a 3D-printed fluidic chemorobotic platform with configurable environments. *Nature Commununications* **8**, 1144, doi:10.1038/s41467-017-01161-8 (2017).
57. te Brinke, E. *et al.* Dissipative adaptation in driven self-assembly leading to self-dividing fibrils. *Nature Nanotechnology* **13**, 849–855, doi:10.1038/s41565-018-0192-1 (2018).
58. Gevers, W., Kleinkauf, H. & Lipmann, F. Peptidyl transfers in gramicidin S biosynthesis from enzyme-bound thioester intermediates. *Proceedings of the National Academy of Sciences of the United States of America* **63**, 1335–1342, doi:10.1073/pnas.63.4.1335 (1969).
59. Kleinkauf, H. & Dohren, H. A nonribosomal system of peptide biosynthesis. *European Journal of Biochemistry* **236**, 335–351, doi:10.1111/j.1432-1033.1996.00335.x (1996).
60. Hnisz, D., Shrinivas, K., Young, R. A., Chakraborty, A. K. & Sharp, P. A. A phase separation model for transcriptional control. *Cell* **169**, 13–23, doi:10.1016/j.cell.2017.02.007 (2017).
61. Chong, S. *et al.* Imaging dynamic and selective low-complexity domain interactions that control gene transcription. *Science* **361**, doi:10.1126/science.aar2555 (2018).

Figures

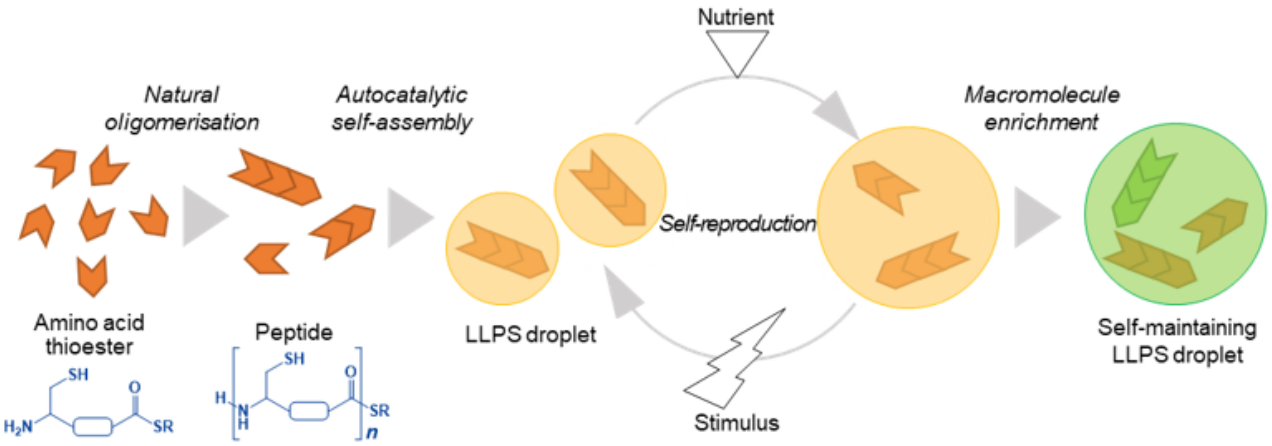

Figure 1

Emergence of proliferating and self-maintaining droplet protocells. In the first stage, the amino acid thioester is oligomerised to produce a peptide. From the product, droplets are formed by liquid-liquid phase separation. By continuously adding amino acid thioester as a nutrient and physical stimulus to the droplets, the formed droplets divide while self-reproducing autocatalytically by incorporating nutrients. The proliferating droplet exhibits self-maintenance properties by concentrating macromolecules such as nucleic acids.

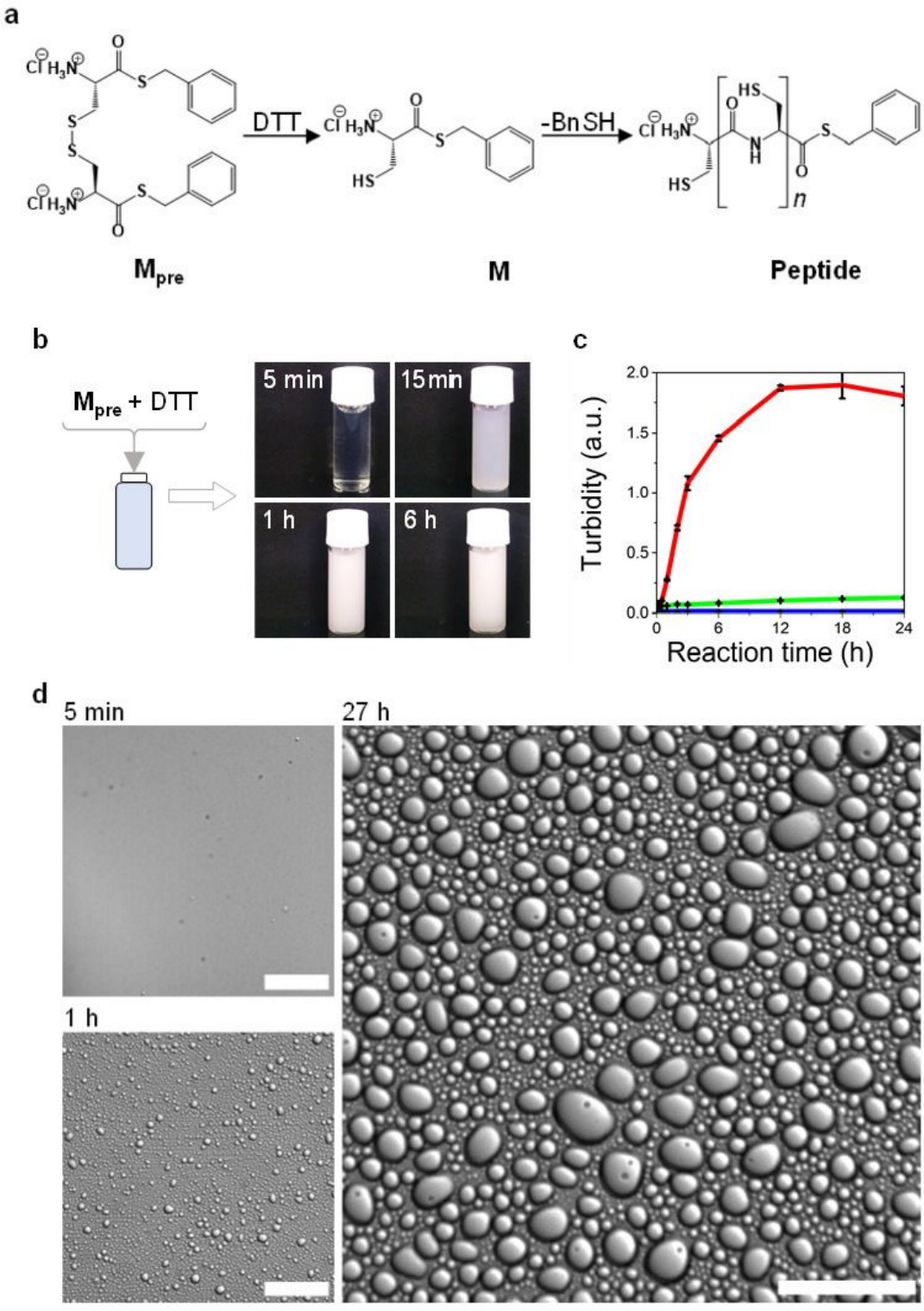

Figure 2

Droplet formation from Mpre and DTT. a, Reduction of the monomer precursor Mpre and oligomerisation of M. b, Preparation of specimens: time-lapse photographs taken after addition of Mpre (10 mM) and DTT (25 mM) to water. c, Change in turbidity after addition of Mpre (10 mM) and DTT (25 mM), either together or individually, to water: red line, Mpre and DTT mixture; green line, aqueous solution of Mpre;

blue line, aqueous solution of DTT (n = 5; error bars indicate standard deviations). d, DIC microscopy images of the solution of Mpre (50 mM) and DTT (125 mM) after mixing. Scale bars represent 40 μm.

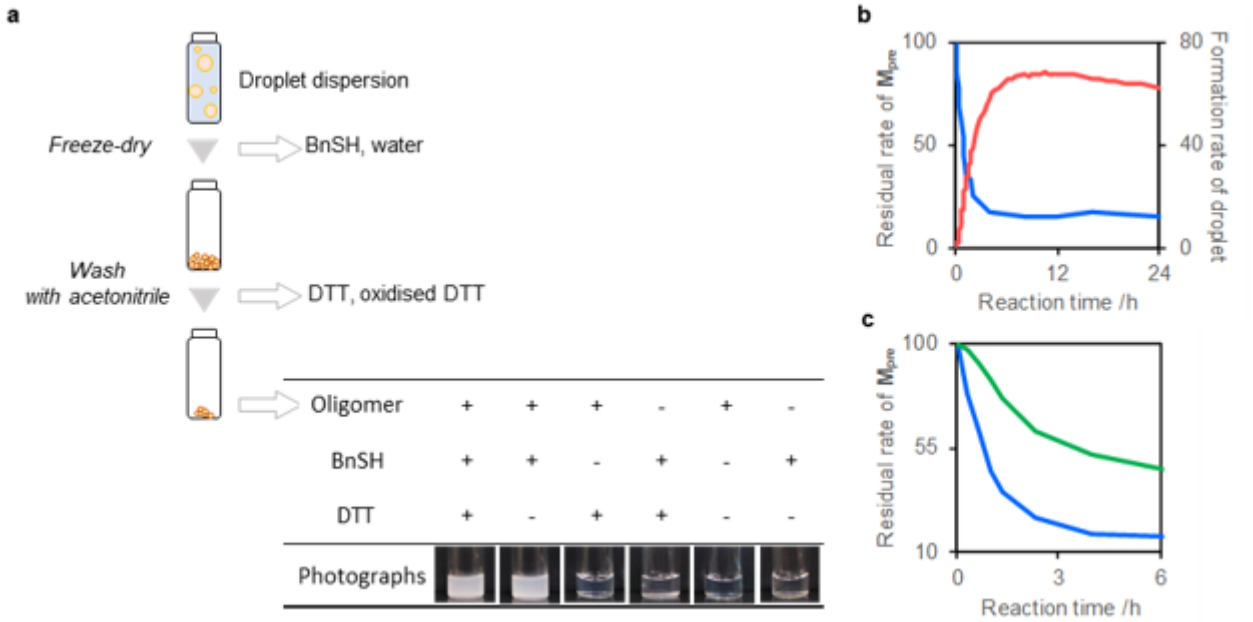

Figure 3

Formation of molecular assemblies induced by oligomerisation. a, Schematic illustration of the separation of oligopeptides from the reaction solution. The table shows the droplet-forming abilities of the obtained oligopeptides with and without BnSH and DTT; +: addition of corresponding reagent, -: no addition of corresponding reagent. The microscopy images are shown in Fig. S11. b, Residual rate of Mpre (blue line) and formation rate of droplets (red line) in a 24 h interval after mixing Mpre (10 mM) and DTT (25 mM). The expanded image of the curve for formation rate of droplets was shown in Fig. S13. c, Residual rate of Mpre in the 6-h interval after mixing Mpre (10 mM) with 25 mM (blue line) and 13 mM (green line) DTT.

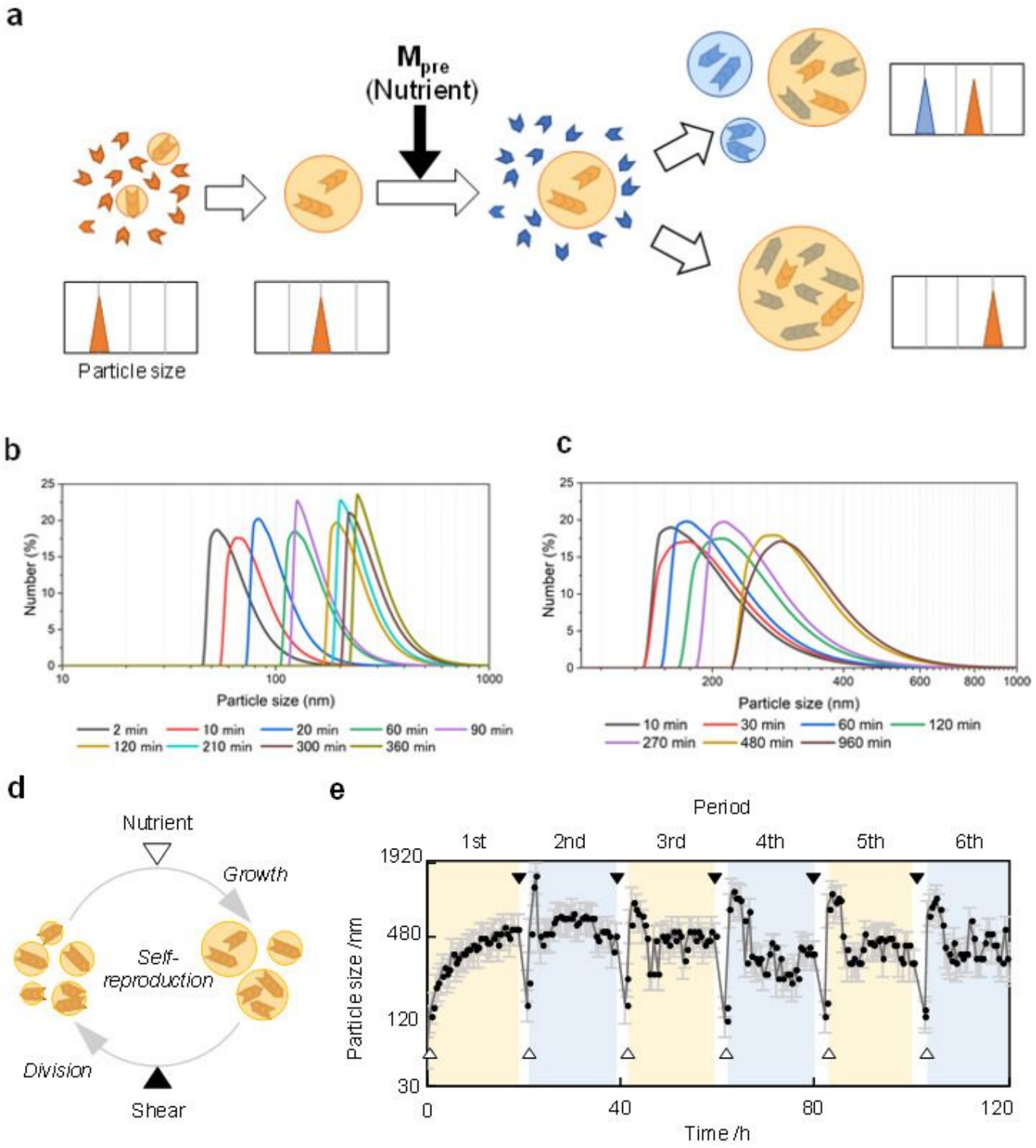

Figure 4

Growth-division cycle of self-reproducing LLPS droplets. a, Schematic particle size distributions after the first and second addition of Mpre (nutrient) and DTT. After the first addition, the particle sizes increase and the corresponding distribution shifts to the right. After the second addition, if the LLPS droplets do not self-reproduce, a new peak centred at a smaller particle size than the original population will appear (upper right). However, if the LLPS droplets self-reproduce, only the original population will be detected,

and the corresponding peak will shift to the right (lower right). b, Particle size distributions measured at different times in the 10 min–24 h interval after addition of Mpre (10 mM) and DTT (25 mM) to water. c, Particle size distributions of the solution after the second addition of Mpre and DTT 24 h after the first addition (the same amounts of Mpre and DTT were added to the solution). Only one population was detected after the second addition. For both b and c, the x-axis refers to the particle size and the y-axis to the percentage of droplets to the normalised droplet population. d, Growth-division cycle of self-reproducing LLPS droplets. LLPS droplets grew upon addition of nutrient (white triangle) and were divided by the applied stimulus (shear, black triangle). e, Time evolution of average particle size upon repeated nutrient addition and stimulus cycles. Twenty hours after addition of nutrient, the dispersion was diluted with an equal amount of water and extruded; immediately after extrusion, the same amount of nutrient originally used was added again. These operations were repeated five times. White triangles, addition of Mpre and DTT; black triangles, extrusion. The raw image was shown in Fig. S17 to visualise the details. Error bars represent standard deviations.

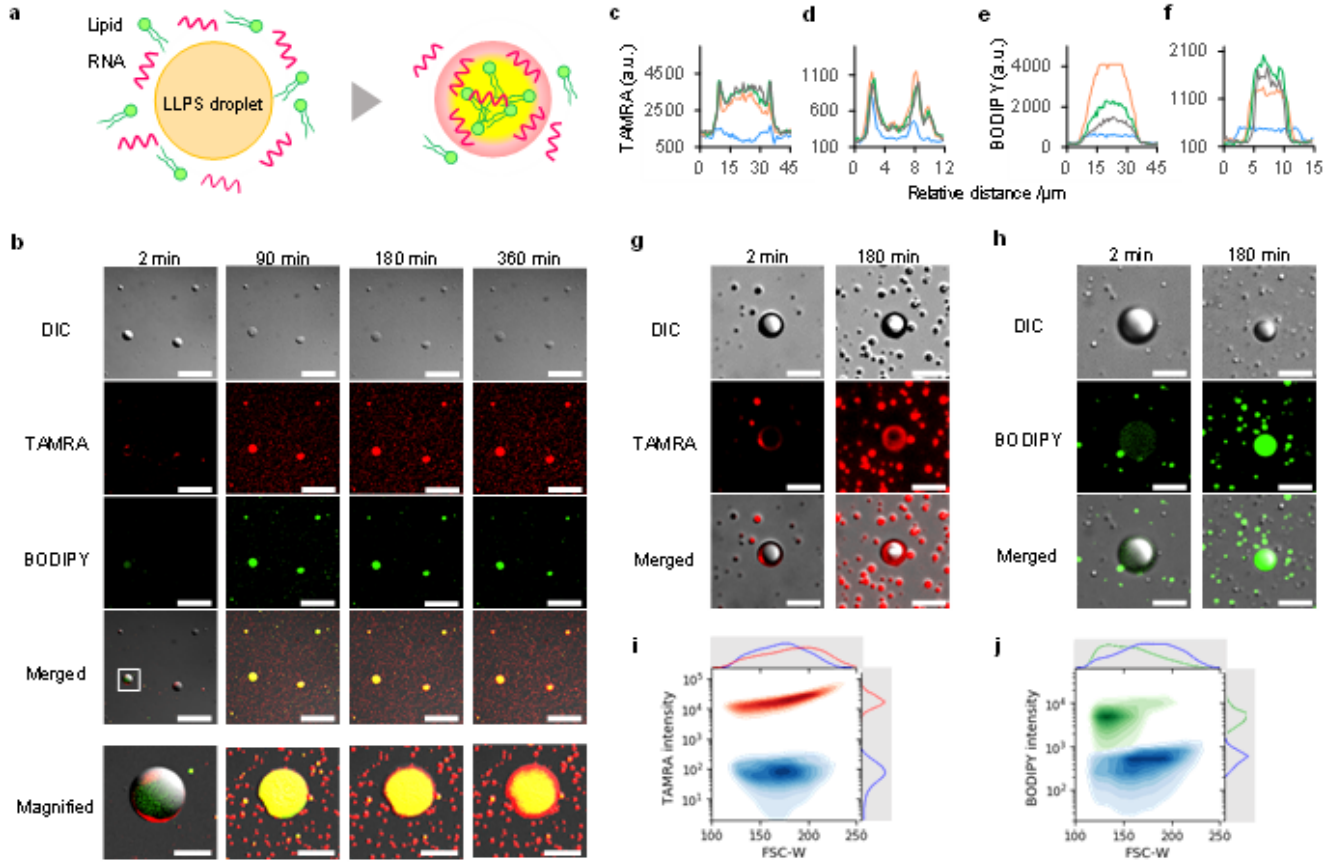

Figure 5

Incorporation, concentration and separation of biological molecules inside LLPS-droplets by internal structural heterogeneity. Concentrated nucleic acids and lipids in LLPS-droplets exhibit new higher-order functions of the droplets. a, Due to the spatial heterogeneity of a LLPS droplet, the RNA and lipids were concentrated and spatially separated, and novel high-order properties that have never been exhibited by the droplet itself could be exhibited. b, CLS fluorescence microscopy images of the LLPS droplet dispersion at 2, 90, 180 and 360 min after addition of the TAMRA-RNA (10 μM) and BODIPY-lipid (10 μM)

solutions; both the individual and merged signals are shown (DIC = differential interference contrast microscopy image). The scale bars of the top four row images are 100 μm, whereas those of the bottom row (magnified) images represent 20 μm. The white rectangle frame in the photo in the merged image shows the magnified image below. (c–f) Time evolution of line profiles of fluorescence intensities along horizontal line through the centre of the LLPS droplet after TAMRA-RNA and BODIPY-lipid addition: blue line, 2 min; yellow line, 90 min; green line, 180 min; black line, 360 min. c, Line profiles of TAMRA-RNA fluorescence intensity of the LLPS droplet shown in the bottom row of Fig. 5b. d, Line profiles of TAMRA-RNA fluorescence intensity of the LLPS droplet shown in Fig. 5g. e, Line profiles of BODIPY-lipid fluorescence intensity of the LLPS droplet shown in the bottom row of Fig. 5b. f, Line profiles of BODIPY-lipid fluorescence intensity of the LLPS droplet shown in Fig. 5h. g, CLS fluorescence microscopy images of the dispersion 2 and 180 min after addition of 1 μM TAMRA-RNA solution. The scale bar represents 20 μm. h, CLS fluorescence microscopy images of the dispersion 2 and 180 min after addition of 1 μM BODIPY-lipid solution. The scale bar represents 20 μm. i, Bivariate kernel density estimation (KDE) analysis applied to the distributions of TAMRA fluorescence intensity and pulse width of forward scatter (FSC-W, corresponding to the particle size) of droplets before and after the addition of TAMRA-DNA. Histograms and scatter plots derived from each droplet before (red) and after (blue) the addition of TAMRA-DNA are shown. The curve on the x-axis shows the histogram of forward scattering intensity and that on the y-axis shows the histogram of TAMRA fluorescence intensity. The number of the measured droplets are 10,000. j, Bivariate KDE of the distributions of BODIPY intensity and FSC-W of droplets before and after the addition of BODIPY-HPC. Darker colours represent higher densities. The univariate KDEs for both variables are also shown in the plot. Histograms and scatter plots derived from each droplet before (red) and after (green) the addition of BODIPY-HPC are shown. The curve on the x-axis shows the histogram of forward scattering intensity and that on the y-axis shows the histogram of BODIPY fluorescence intensity. The number of the measured droplets are 10,000. RNase-free water was used for all RNA and control experiments.

Supplementary Files

This is a list of supplementary files associated with this preprint. Click to download.

- SupplementaryMovie1.mp4
- SupplementaryMovie2.mp4
- SIver2fin.docx